Results in Physics 6 (2016) 690–697

Contents lists available at ScienceDirect

Results in Physics

journal homepage: www.journals.elsevier.com/results-in-physics

# Experimental study on the stress corrosion cracking behavior of AISI347 in acid chloride ion solution ☆

Yanpeng Qu, Runkun Wang, Chao Wang, Songying Chen *

*Key Laboratory of High-efficiency and Clean Mechanical Manufacture, School of Mechanical Engineering, Shandong University, Jinan 250061, PR China*

ARTICLE INFO

*Article history:*
Received 18 August 2016
Received in revised form 18 September 2016
Accepted 25 September 2016
Available online 30 September 2016

*Keywords:*
Stress corrosion cracking
Chloride ion
Slow strain rate testing
AISI347

ABSTRACT

The stress corrosion cracking (SCC) behavior of AISI347 austenitic stainless steel exposed to acid solution containing chloride ion at different temperature and pressure is studied through slow strain rate testing (SSRT) at different test condition. The result of SSRT shows, with the pressure increasing, the SCC resistance is getting worse and the trend of brittle fracture presented by the fracture surface is more obvious. With the temperature rising, the mechanical properties of AISI347 getting worse first and then getting better, it gets to be the worst when the temperature is 260 °C. The result of significance effect analysis of temperature and pressure on SCC shows that the temperature has a greater effect on the resistance to SCC of AISI347 austenitic stainless steel than the pressure. The main component of passive film is analyzed and the mechanism of SCC is discussed. Chromium oxides soluble in the acidic chloride solution results in the forming of corrosion pits and the cracking of the passive film under stress.



## Introduction

Stainless steels are often perceived as the backbone of modern industry [1]. AISI347 austenitic stainless steel is widely utilized in components design for high temperature applications such as nuclear reactors, boilers and chemical units for their high corrosion resistance and good mechanical properties [2–6]. Some of the hydrogenation desulfurization device, water vapor of the bill unit, acidic water heat exchanger tube bundle, industrial boiler in coastal field and high $Cl^-$ water area are made by AISI347 austenitic stainless steels [7]. The excellent corrosion resistance of austenitic stainless steel benefits from the presence of a thin oxide passive film on the metal surface [8–10]. Stress corrosion cracking (SCC) is one of the major failure modes to which austenitic stainless steel are subjected to [11]. There are many kind of theories to explain the SCC of austenitic stainless steel happens, but only two of them are accepted by the most scientific scholars. One is the passive film damage theorem and another is the adsorption theory [12,13]. The electrochemical reaction is the basis of the two theories. The existence of passive film improves the corrosion resistance of stainless steel. Studies have pointed out that the passive film is mainly made up of chromium oxide ($Cr_2O_3$) [14,15]. Chandra et al. [16] investigated the microstructure and electrochemical characterization of heat-treated AISI347 stainless steel by ageing at 650 °C and 750 °C. Yoo et al. [17] researched the effects of the carbon and nitrogen contents of AISI347 in the light of the microstructure and microscopic fracture behavior. Ramesh et al. [18] studied the cyclic deformation behavior during thermo-mechanical fatigue (TMF) and isothermal fatigue (IF) testing in air. However, less attention has been paid to the effects of temperature and pressure on stress corrosion cracking of AISI347 exposed to acid solution containing chloride ion. A project was therefore initiated to investigate the mechanical properties and microstructure of AISI347 exposed to acidic chloride solution at high temperature and pressure.

In this study, the test apparatus of slow strain rate test system (SERT-5000- D9H, Toshin Co. Ltd.) is employed to perform the SSRT experiments, measuring the test parameters of AISI347, simulating the high temperature and pressure environment with acid $Cl^-$, exploring the regular of the stress corrosion cracking resistance in different environment, and studying the mechanism of the SCC through analyzing the corrosion products on the fracture surface of the specimen.

## Experiments

### *Material and specimens preparation*

The investigated material was portion of commercial AISI347 austenitic stainless steel. The mechanical properties and the chem-

☆ This project is supported by Science and Technology Development Planning of Shandong Province, China (2014GGX108001).

* Corresponding author.
*E-mail address:* chensy66@sdu.edu.cn (S. Chen).

http://dx.doi.org/10.1016/j.rinp.2016.09.014
2211-3797/

**Table 1**
Mechanical property of AISI347.

| Tensile strength $\sigma_b$ (MPa) | Yield strength $\sigma_s$ (MPa) | Tensile elongation $\delta$ (%) | Hardness HRC |
|---|---|---|---|
| 520 | 205 | 35 | 90 |

**Table 2**
Chemical components of AISI347.

| Element type | C | Si | Mn | Ni | Cr | Nb |
|---|---|---|---|---|---|---|
| Amount (%) | 0.08 | 1.00 | 2.00 | 11.13 | 18.08 | 0.42 |

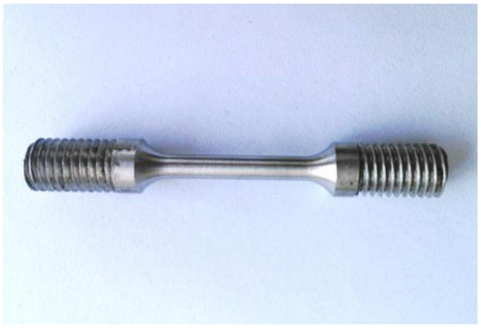

**Fig. 1.** Specimen for SSRT.

ical components of the material are shown in Tables 1 and 2, respectively. Seven groups of specimens were prepared for SSRT and three parallel samples were set in each group. The images of the specimen were shown in Fig. 1. The dimensions of the specimen for SSRT were shown in Fig. 2. Before experiment, no thermal treatment was applied to the samples.

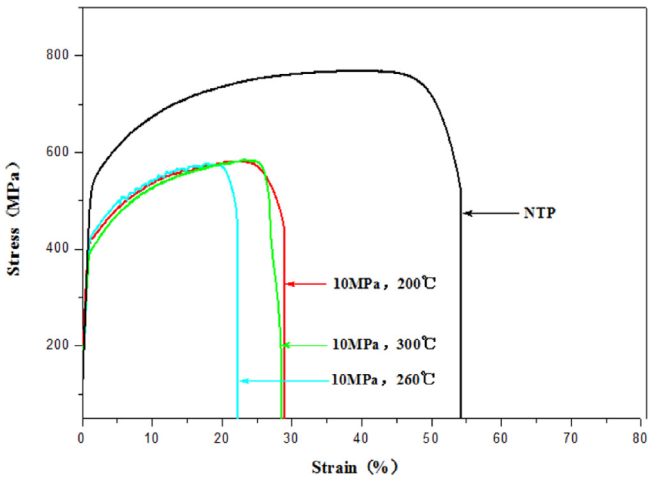


**Fig. 3.** Slow tensile curves of AISI347 at NTP and 10 MPa with different temperatures.

According to NACE TM-0198/TM-0177, the smoother of the surface is, the stronger the corrosion resistant ability of the stainless steel gets [19]. So, the specimen surface is ground with silicon carbide papers from grit 240, 400 and 800 successively till no scratches on the surface, then rinsed with deionized water, ethanol and dried with a hair drier.

*Slow strain rate tests*

SSRT is stretching the specimen immersed in a specific solution by tensile testing machine at a constant rate till it was fractured. The test is performed according to NACE TM-0198/TM-0177. AISI347 austenitic stainless steel is widely used to make super

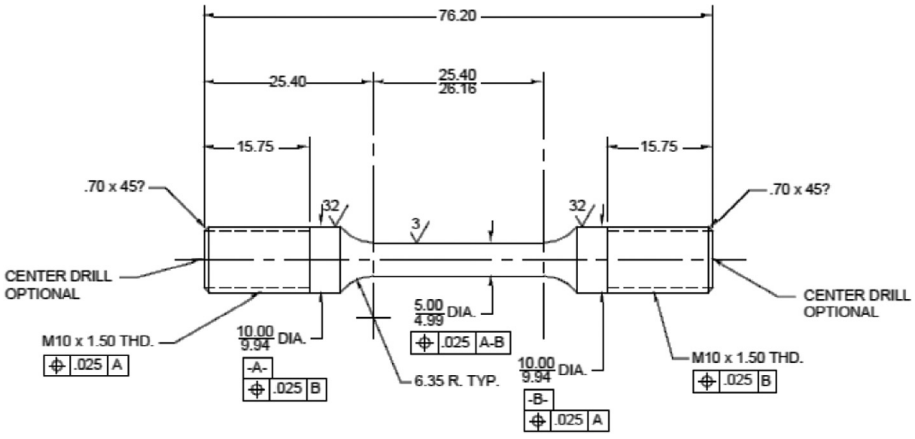


**Fig. 2.** The dimensions of the specimens for SSRT.

**Table 3**
Experimental environment, rate of extension and dimensions of specimens for SSRT.

| Specimen | Type | Pressure (MPa) | Temperature (°C) | Gauge length (mm) | Diameter (mm) | Rate of extension 1/s | Environment |
|---|---|---|---|---|---|---|---|
| A | AISI347 | 10 | 200 | 25 | 4.48 | $2.0 \times 10^{-6}$ | NACE A |
| B | AISI347 | 10 | 260 | 25 | 4.41 | $2.0 \times 10^{-6}$ | NACE A |
| C | AISI347 | 10 | 300 | 25 | 4.42 | $2.0 \times 10^{-6}$ | NACE A |
| D | AISI347 | 0 | 20 | 25 | 4.96 | $2.0 \times 10^{-6}$ | $N_2$ |
| E | AISI347 | 16 | 200 | 25 | 4.97 | $1.5 \times 10^{-6}$ | NACE A |
| F | AISI347 | 16 | 260 | 25 | 4.96 | $1.5 \times 10^{-6}$ | NACE A |
| G | AISI347 | 16 | 300 | 25 | 4.97 | $1.5 \times 10^{-6}$ | NACE A |

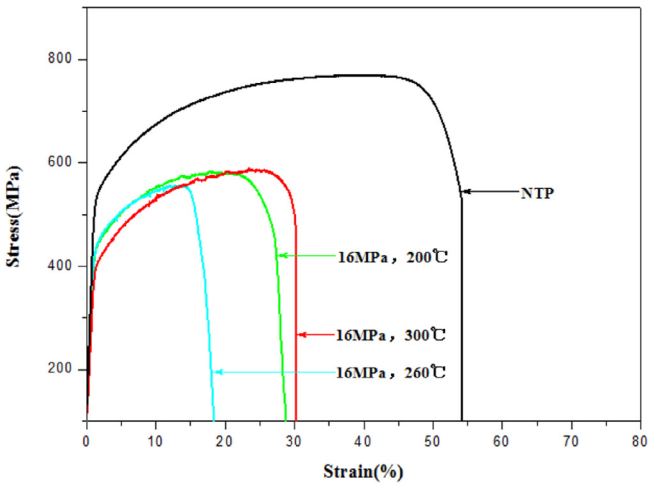


**Fig. 4.** Slow tensile curves of AISI347 at NTP and 16 MPa with different temperatures.

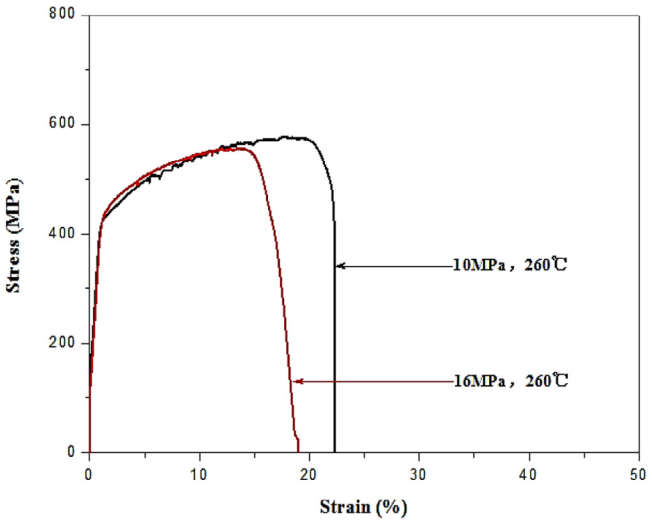


**Fig. 6.** Slow tensile curves of AISI347 at 260 °C with different pressures.

**Table 4**
Stress corrosion sensitivity index.

| Type | Test condition | Tensile strength ($\sigma$/MPa) | Elongation ($\delta$/%) | Inner product power ($A$/MPa) | Sensitivity index | | |
|---|---|---|---|---|---|---|---|
| | | | | | F ($\sigma$)/ % | F($I$)/ % | F ($A$)/ % |
| AISI347 | NTP($N_2$) | 769.1 | 54.2 | 38358.1 | – | – | – |
| AISI347 | 10 MPa 200 °C | 581.6 | 29.1 | 15274.3 | 24.4 | 46.3 | 60.2 |
| AISI347 | 10 MPa 260 °C | 576.2 | 22.3 | 11576.6 | 25.1 | 58.9 | 69.8 |
| AISI347 | 10 MPa 300 °C | 585.5 | 28.5 | 14554.1 | 23.9 | 47.4 | 62.1 |
| AISI347 | 16 MPa 200 °C | 583.6 | 28.7 | 14858.5 | 24.1 | 47.0 | 61.3 |
| AISI347 | 16 MPa 260 °C | 550.7 | 18.9 | 8866.9 | 28.4 | 65.1 | 76.9 |
| AISI347 | 16 Mpa 300 °C | 588.3 | 30.3 | 15948.8 | 23.5 | 44.1 | 58.4 |

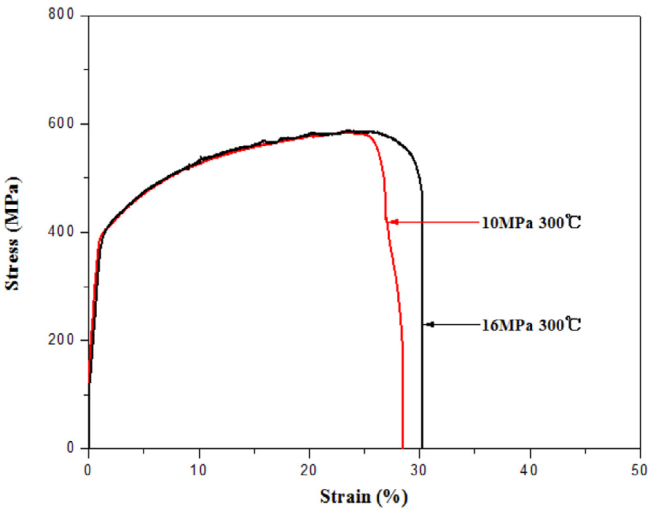


**Fig. 7.** Slow tensile curves of AISI347 at 300 °C with different pressures.

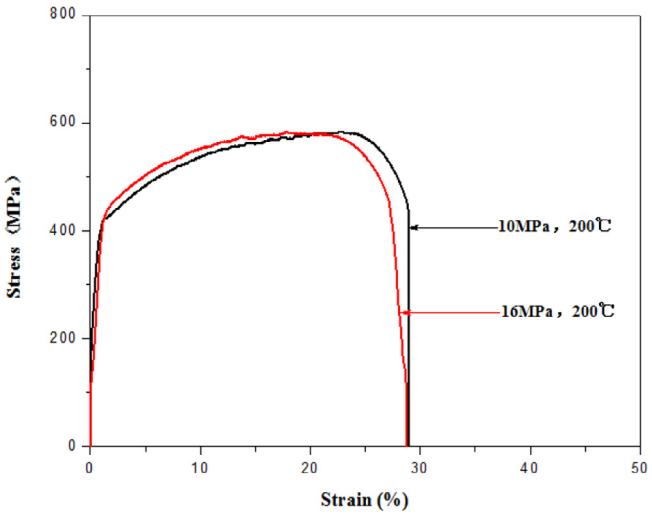


**Fig. 5.** Slow tensile curves of AISI347 at 200 °C with different pressures.

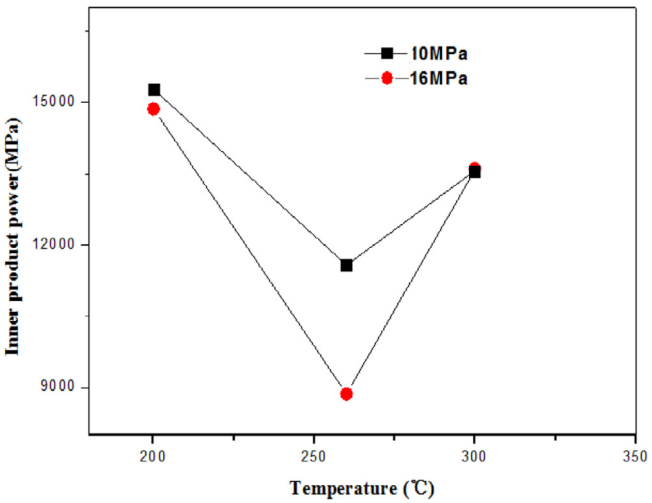


**Fig. 8.** The inner product power of AISI347.

**Table 5**
The result of correlation coefficient.

| $k$ | $\gamma_1(k)$ | $\gamma_2(k)$ |
|---|---|---|
| 1 | 0.63 | 0.67 |
| 2 | 0.43 | 0.96 |
| 3 | 0.57 | 0.52 |
| 4 | 0.45 | 0.64 |
| 5 | 1.00 | 0.63 |
| 6 | 0.41 | 0.45 |
| $\bar{\gamma}$ | 0.58 | 0.65 |

heater, re-heater, steam pipe and heat exchanger. According to the actual working conditions, seven groups of specimens in different environment are tested in this test.

The specimens were soak in NACE A solution (5%NaCl + 0.5% $CH_3COOH$ + Deionized Water) and kept in a closed autoclave. Temperature is controlled by a heating jacket and the pressure is adjusted by putting into $N_2$. The specimens were stretched at a constant rate. The test environment, rate of extension and the actual dimensions of these specimens are shown in Table 3. The test conditions regarding pressure and temperature are set to simulate the industrial process environment which the material are involved in manufacturing the furnace tubes, heat exchanger tubes in petrochemical industries. The force and elongation was detected by the detection system during the deformation.

### *SEM-EDS*

After the SSRT, the scanning electron microscope (SEM) is used to examine the fracture of the specimens to get the morphologies. The energy disperse spectroscopy (EDS) is used to detect the chemical components of the fracture surface.

## Results and discussion

### *Stress strain curves*

In this section, three specimens are repeatedly tested in each experimental group for a more accurate result. Stress corrosion

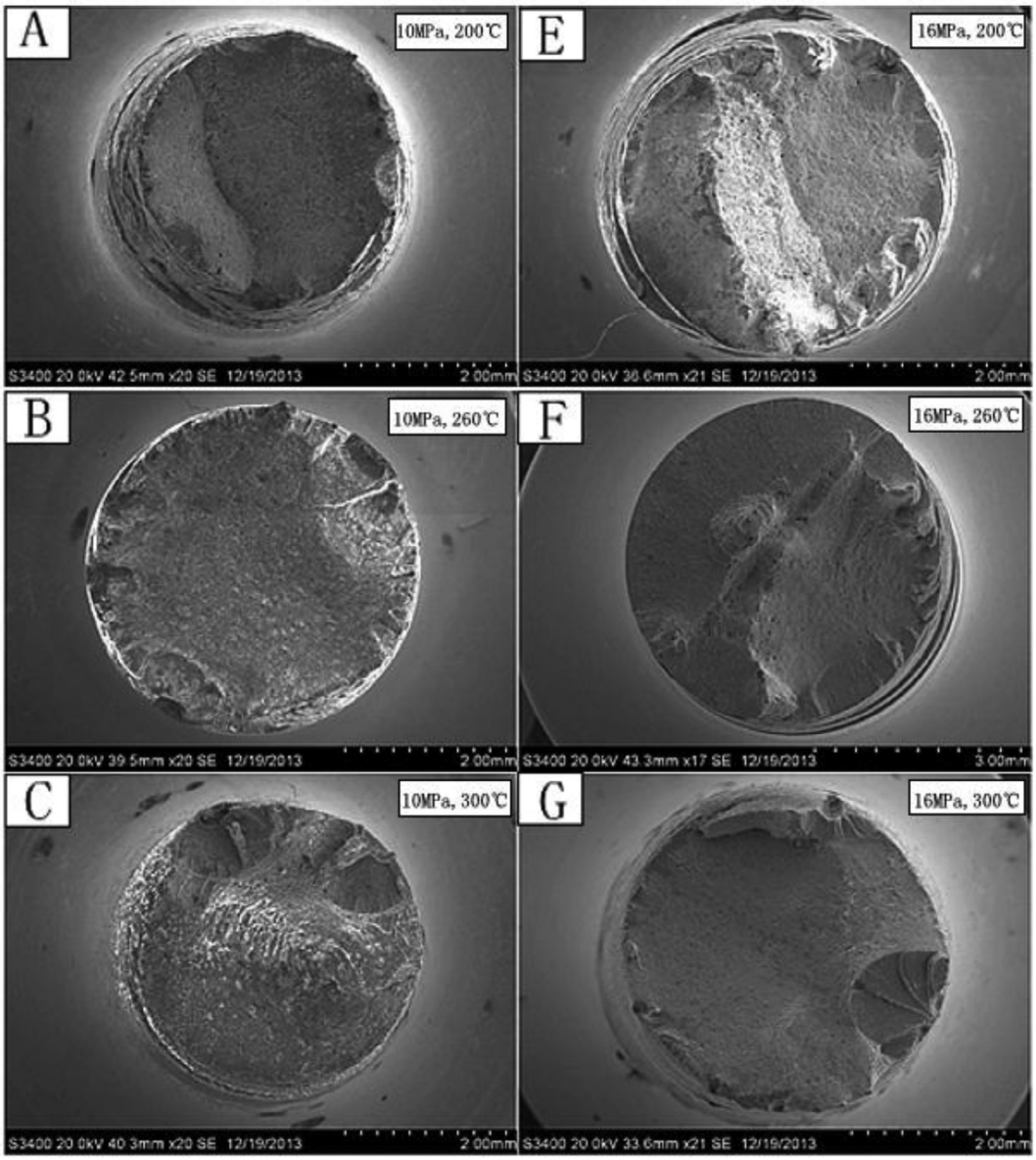


**Fig. 9.** SEM image of AISI347 after SSRT in different environment. Specimen A (A), specimen B (B), specimen C (C), specimen E (E), specimen F (F), specimen G (G).

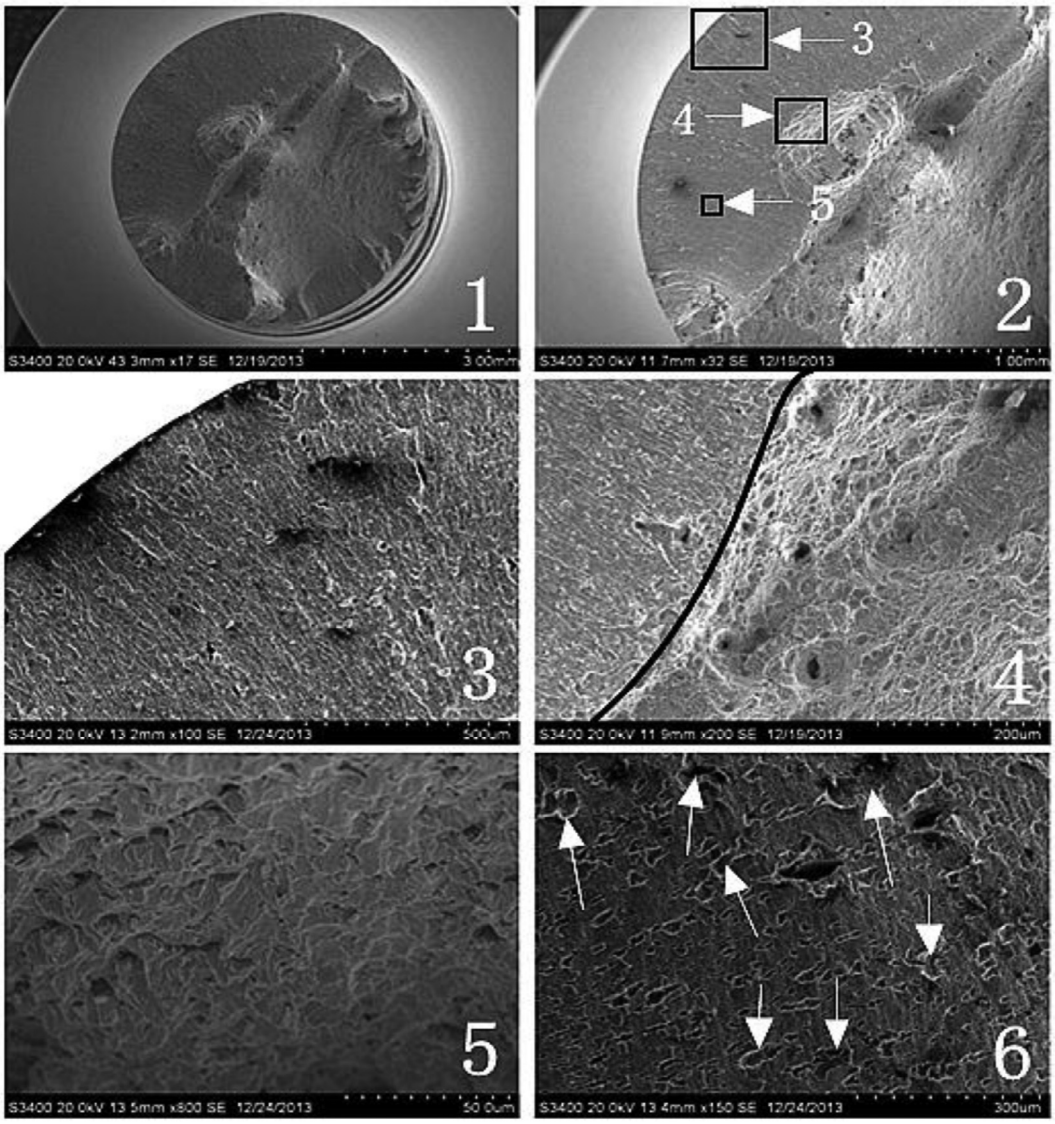


**Fig. 10.** SEM images of specimen F.

sensitivity is evaluated by the relative inner product power F($A$) which is obtained by multiplying from the stress and strain, relative tensile strength F($\sigma$) and relative elongation F($I$) which are defined as follows:

$$F(A) = (A_0 - A)/A_0 \times 100\% \quad (1)$$

$$F(\sigma) = (\sigma_0 - \sigma)/\sigma_0 \times 100\% \quad (2)$$

$$F(I) = (I_0 - I)/I_0 \times 100\% \quad (3)$$

where, $A_0$ represents the integrated area under the tensile curve, named the inner product power, $\sigma_0$ and $I_0$ denotes tensile strength, elongation of the specimen exposed to the inert gas at normal temperatures and pressures (NTP), respectively. $A$, $\sigma$ and $I$ is the corresponding properties at different environment, respectively. The higher of the value is, the greater the stress corrosion sensitivity of the material reaches.

As it is shown in Figs. 3, 4 and Table 4, the SCC sensitivity of AISI347 is declined sharply when in the NACE A solution than in the $N_2$ at normal temperature and pressure (NTP). When the pressure is 10 MPa, the tensile strength, elongation and the inner product power gradually reduced as the temperature increased. When the temperature reaches 260 °C, the mechanical properties all decreased, the tensile strength reaches 576.2 MPa, the elongation reaches 22.3% and the inner product power reaches 11576.6 MPa. As the temperature goes up, they all increased. When the pressure is 16 MPa, it presents the same regular. So the stress corrosion sensitivity is the worst when the temperature is 260 °C. Besides, the sensitivity index shows that, when the temperature is 260 °C and the pressure is 16 MPa, it reaches the highest: F($\sigma$) = 28.4%, F($I$) = 65.1%, F($A$) = 76.9%.

As it is shown among Figs. 5–8, at the early stages of the SSRT, the curves are highly consistent. At the end of the elastic deformation, the two curves separate from each other. The difference between the two curves is apparent when the temperature is 260 °C. The SCC sensitivity of AISI347 at 16 MPa is lower than it at 10 MPa. It indicates that the SCC resistance gets to be the worst when the temperature reaches 260 °C.

*Significance effect analysis of temperature and pressure on SCC*

In consideration of the cost, the data got from the SSRT is too less to pick out which is the major factor of temperature and pressure that affect the result of SCC. So, choosing the appropriate anal-

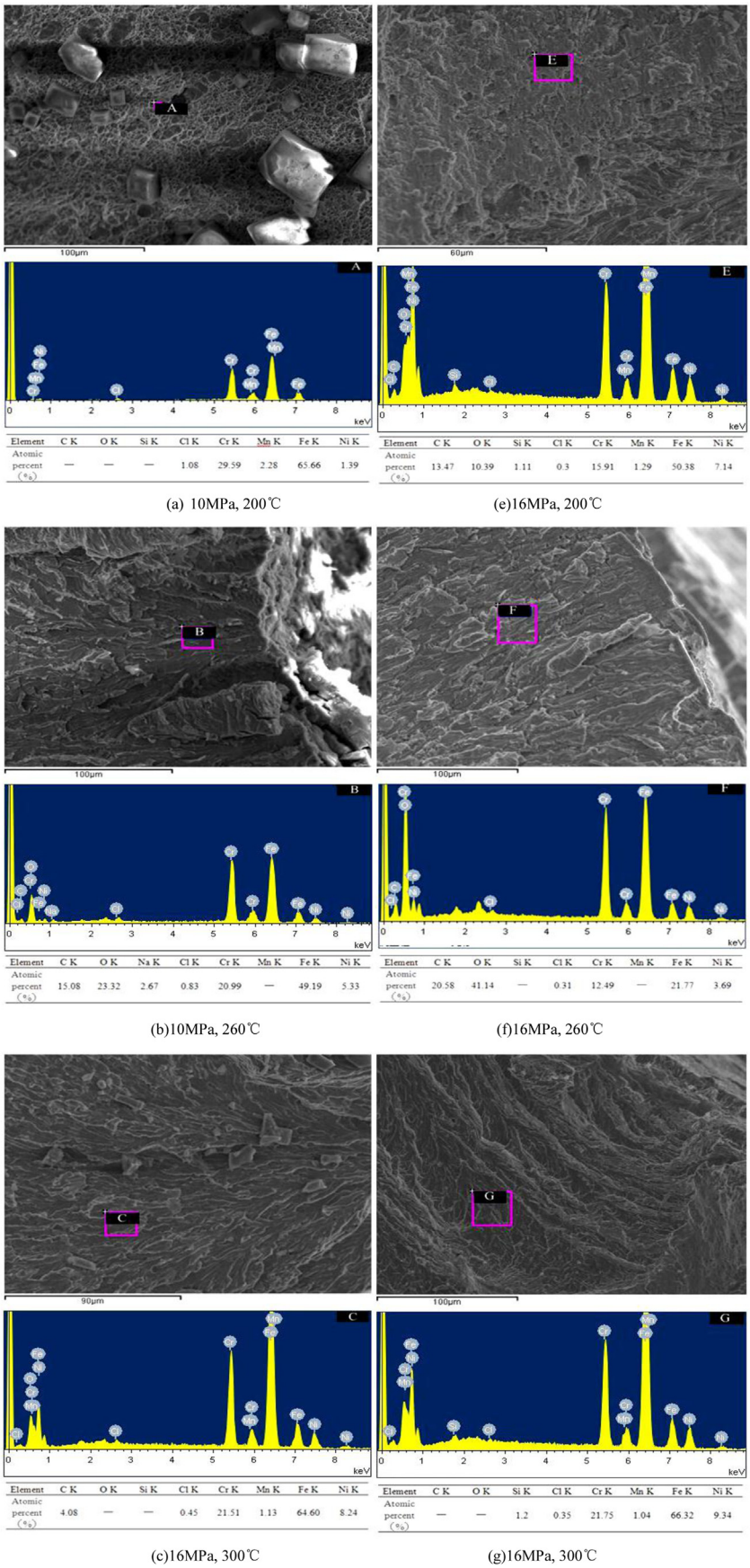


**Fig. 11.** Energy-Spectrum Frequency on the fracture surface of the specimens. (a) Specimen A, (b) Specimen B, (c) Specimen C, (e) Specimen E, (f) Specimen F, (g) Specimen G.

ysis method is very important. Gray system theory [19] is adopted to analysis significance effect of the temperature and pressure on the SCC.

As the following Eq. (4) shows, factors (pressure and temperature) affecting the SCC resistance of austenitic stainless steel are used as comparison sequence $X_1$ and $X_2$, respectively.

$$\begin{aligned} X_1 &= [x_1(1), x_1(2), x_1(3), x_1(4), x_1(5), x_1(6)] \\ X_2 &= [x_2(1), x_2(2), x_2(3), x_2(4), x_2(5), x_2(6)] \end{aligned} \tag{4}$$

The sensitivity index F($A$) is used as reference sequence $X_0$ just as following formula (5) shows.

$$X_0 = [x_0(1), x_0(2), x_0(3), x_0(4), x_0(5), x_0(6)] \tag{5}$$

Because of different unit of the factors, according to the formulae (6) and (7), data are converted into proper dimensionless indexes first.

$$X_0' = \frac{X_0}{\frac{1}{6}\sum_{k=1}^{6} x_0(k)} \tag{6}$$

$$X_i' = \frac{X_i}{\frac{1}{6}\sum_{k=1}^{6} x_i(k)}, \quad i = 1, 2 \tag{7}$$

In order to further analysis the significant effect of the pressure and temperature on the SCC, the relational coefficients that can reflect the degree of association between the comparison sequence and the reference sequence is adapted. The lager of the relational coefficients are, the more closer of the two sequences become.

The absolute difference of the comparison sequence and the reference sequence is obtained by:

$$\Delta_i(k) = \left| x_0'(k) - x_i'(k) \right|, \quad k = 1 \sim 6 \tag{8}$$

The range is calculated by the formula (9).

$$\begin{aligned} M &= \max_i \max_k \Delta_i(k) \\ m &= \min_i \min_k \Delta_i(k) \end{aligned} \tag{9}$$

The correlation coefficients $\gamma_i(k)$ (i = 1, 2) are got from the following Eq. (10).

$$\gamma_i(k) = \frac{m + \xi M}{\Delta_i(k) + \xi M} \tag{10}$$

where $\gamma_1$ (k) and $\gamma_2$ (k) denotes the pressure and temperature correlation coefficient, respectively. $\xi$ is identification coefficient and takes 0.5 here according to the general law. The result of correlation coefficients as Table 5 shows, where $\bar{\gamma}$ is the averaged $\gamma_i$.

From the above table, general speaking, it is easy to see that the correlation coefficient of temperature is higher than pressure. It indicates that the temperature has a greater effect on the resistance to SCC of AISI347 austenitic stainless steel than the pressure.

*Behaviors of SEM and EDS analysis*

As it is shown in Fig. 9, the necking phenomenon of the specimens is inconspicuously while the pressure rises from 10 MPa to 16 MPa. When the temperature reaches 260 °C, it presents obvious characteristics of brittle fracture on the fracture surface. The resistance to SCC of the material reflected by the behaviors of SEM inosculates with the results got from the stress-strain curves.

As it is shown in Fig. 10, Photo 3 and Photo 5 shows that the edge of the fracture surface has appeared mixed-rupture characteristics of trans-granular corrosion and quasi-cleavage. Photo 4 shows that a lot of dimples exist in the interior of the surface (the right of the black line). It indicates that there is no stress corrosion but ductile fracture in this area. Photo 6 shows that many corrosion pits (see arrow) are found on the surface of the profile near the fracture. Corrosion pit is the origin of the SCC [20,21]. So these corrosion pits are the origin of the cracking. These could be explained by the passive film damage theorem. The weak area of the passive film is first be corroded to the form the corrosion pit. Then the crack appears around the corrosion pit and extending along the direction perpendicular to the stress.

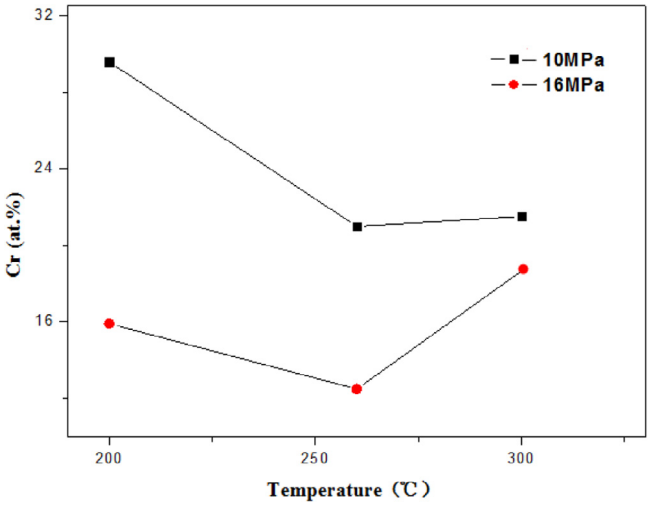


**Fig. 12.** Percent of Cr on the fracture surface of the specimens.

Fig. 11 shows that the detected level of Cr on the edge of the fracture surface is changed with the temperature and pressure. When the pressure is 10 MPa, the level of Cr increases as the temperature goes down. When the temperature reaches 260 °C, it is 20.99 which is the lowest, and it goes up while the temperature continues to rise. When the pressure is 16 MPa, it presents the same regular. It also shows that the higher the pressure is, the lower of the level of Cr is. As it is shown in Fig. 12, the regular of the distribution level of Cr is agreed with materials' sensitivity. Chromium oxide ($Cr_2O_3$) is the main component of passive film. The passive film damage theorem indicated that a new layer of passive film formed after the original passive film rupture. So it could speculate that temperature and pressure have large effect on the dissolution of Chromium oxides in the NACE A solution. Chromium oxides soluble in the solution result in the cracking of the passive film and the forming of corrosion pits.

## Conclusions

The results of this research suggest the following conclusions:

(1) Temperature and pressure has a great influence on corrosion resistance of AISI347 exposed to NACE A solution. The stress corrosion sensitivity of AISI347 at 16 MPa is lower than it at 10 MPa. The trend of brittle fracture presented by the fracture surface is more significant. With the temperature rising, the mechanical properties of AISI347 getting worse first and then getting better, it gets to be the worst when the temperature is 260 °C. When the temperature reaches 260 °C, the sensitivity index is the largest.
(2) The temperature has a greater effect on the resistance to SCC of AISI347 austenitic stainless steel than the pressure.
(3) Chromium oxides soluble in the NACE A solution lead to the cracking of the passive film and the forming of corrosion pits.

## Acknowledgements

The authors acknowledge the Project (2014GGX108001) supported by the Science and Technology Development Planning of Shandong Province, China. Besides, the authors would like to express their thanks to Qingdao Academy of Safety Engineering for supplying the help on the SSRT.

## References

[1] Khatak HS, Baldev R. Corrosion of austenitic stainless steels: mechanism, mitigation and monitoring. ASM International Narosa Publishing House; 2002.
[2] Guan K, Xu X, Xu H, Wang Z. Nucl Eng Des 2005;235:2485–94.
[3] Kallqvist J, Andren HO. Mater Sci Eng A 1999;270:27–32.
[4] Yae Kina A, Souza VM, Tavares SSM, Souza JA, de Abreu HFG. J Mater Process Technol 2008;199:391–5.
[5] Moura V, Kina Aline Y, Tavares SSM, Lima LD, Mainier FB. J Mater Sci 2008;43:536–40.
[6] Zinkle SJ, Was GS. Materials challenges in nuclear energy. Acta Mater 2013;61:735–58.
[7] Mao-dong LI, Lin YANG, Yu-hui DU. Present situation of corrosion caused by $Cl^-$ ion and countermeasure in industrial boilers. Total Corros Control 2008;5 (22):33–5.
[8] Olsson C-OA, Landolt D. Passive films on stainless steels/chemistry, structure and growth. Electrochim Acta 2003;48:1093–104.
[9] Desestret A, Charles J. Les aciers inoxydables. Les Ulis, France: Editions de Physiques; 1990. p. 631.
[10] Josefsson B, Nilsson JO, Wilson A. Proc. duplex stainless steel, Beaune, Bourgogne, France, Oct 28–30, 1991. Los Ulis, France: Editions de Physiques; 1992. p. 67.
[11] Mine Y, Kimoto T. Hydrogen uptake in austenitic stainless steels by exposure to gaseous hydrogen and its effect on tensile deformation. Corros Sci 2011;53:2619–29.
[12] Marcus P, Maurice V, Strehblow HH. Localized corrosion (pitting): a model of passivity breakdown including the role of the oxide layer nanostructure. Corros Sci 2008;50:2698–704.
[13] Pan Ying, Zhang San-ping, Zhou Jian-long, Li Xiao-gang. Research progress of pitting corrosion initiation of metal materials. Equip Environ Eng 2010;7 (4):67–71.
[14] Montemor MF, Ferreira MGS, Hakiki NE, Da Cunha Belo M. Chemical composition and electronic structure of the oxide films formed on 316L stainless steel and nickel based alloys in high temperature aqueous environments. Corros Sci 2000;42:1635–50.
[15] Li Jin-bo, Zheng Mao-sheng, Zhu Jie-wu. Semi-conductive properties of passive film formed on 304L stainless steel. Corros Sci Prot Technol 2006;18 (5):348–52.
[16] Chandra K, Kain Vivekanand, Tewari R. Microstructural and electrochemical characterization of heat-treated 347 stainless steel with different phases. Corros Sci 2013;67:118–29.
[17] Yoo One, Oh Yong-Jun, Lee Bong-Sang, Nam Soo Woo. The effect of the carbon and nitrogen contents on the fracture toughness of type 347 austenitic stainless steels. Mater Sci Eng A 2005;405:147–57.
[18] Ramesh Mageshwaran, Leber Hans J, Janssens Koenraad GF, Diener Markus, Spolenak Ralph. Thermomechanical and isothermal fatigue behavior of 347 and 316L austenitic stainless tube and pipe steels. Int J Fatigue 2011;33:683–91.
[19] Liu Sifeng, Lin Yi. Grey systems, vol. 68. Springer; 2011. pp. 1–18.
[20] Hong T, Nagumo M. Effect of surface roughness on early stages of pitting corrosion of type 301 stainless steel. Corros Sci 1997;39:1665–72.
[21] Yan LI, Kewei FANG, Feihua LIU. Influence of $Cl^-$ on development behavior from pitting corrosion to stress corrosion cracking of 304L stainless steel. Corros Prot 2012;33(15):955–9.